DOI: 10.61782/fa.2023.0344

forum acusticum 2023

# WIND TUNNEL TESTING OF MICRO-PERFORATED MATERIALS

**Cedric Maury**[1] **Teresa Bravo**[2*]
[1] Aix Marseille Univ, CNRS, Centrale Marseille, Marseille, France
[2] Spanish National Research Council (CSIC), Spain

## ABSTRACT

Micro-perforated liners can be of interest for the attenuation of the low-frequency noise in ducted geometries that can appear for instance due to the presence of a Turbulent Boundary Layer (TBL) excitation that contributes to the noise between 500 Hz and 2 kHz. Classical acoustic liners are locally-reacting devices constituted of perforates rigidly-backed by a honeycomb filled cavity. An alternative approach for reducing wall-friction in aero-acoustic applications is the use of facesheets with sub-millimetric diameter perforations. In this study, we perform a cost-efficient experimental characterization for comparing the performance of micro-perforated partitions with those of fibrous non-resonant absorbers for the attenuation of acoustic waves and flow-induced noise in a low-speed wind tunnel. Two types of excitations have been studied, a fully-developed TBL and a source-induced noise using flush-mounted compression drivers. We have used a nosecone microphone system for the determination of velocity and intensity profiles above the micro-perforated and fibrous test sections. The results obtained showed that the sound pressure levels and intensity fluxes in the proximity of the wall-treatments present important modifications when considering micro-perforated panels at the cavity resonance.

**Keywords:** *flow-induced noise, microperforates, turbulent boundary layer.*

[*] ***Corresponding author***: *teresa.bravo@csic.es*


## 1. INTRODUCTION

The generation of noise as a consequence of the interaction between an airframe surface and a mean flow has been widely analyzed due to the large number of applications and its importance in real-life problems. For instance, the noise between the exhaust flow of a jet and the surface of the trailing-edge is a great concern in the transportation systems [1]. These flow-induced noise problems will become more prominent in the near future, especially in the aeronautical sector due to the development of ultra-high bypass ratio engines, as the distance between the turbofan and the airframe surfaces and lifting devices will be relocated and reduced [2].

Considering the energy sector, flow-induced noise is generated for instance by the impingement of the turbulent boundary layer onto the wind-turbine blades [3]. This problematic of noise emissions due to clean technologies such as wind-turbines will become progressively more important. Indeed, windfarms will be further developed in order to reach the "Net Zero" roadmap objectives set by the European Union for clean energy transition, but may be restricted by their visual impact and noise footprint. Concerning the field of building acoustics, one challenge is the design of facade openings, such as apartment windows that would let entering an air flow to ensure regular ventilation of the dwellings while protecting the occupants from external noise pollution [4]. This problem is particularly present in urban areas and near transportation routes. In hot zones, these natural ventilation systems allow also to ensure a minimum level of thermal comfort.

In order to maintain interior comfort for temperature and humidity, an alternative is the operation of air-conditioning and mechanical ventilation systems installed in buildings that also represent noise pollution and energy comsumption. The characterisation [5] and control of ducted fan noise sources is a recursive area of research considering not only the sound power radiated during the use of the appliance, but also the electricity comsumption.

Primary passive techniques include modification of fan blades to radiate lower noise emission. Concepts proposed for flow-induced noise reduction include trailing edge serrations [6], low-noise airfoil designs [7], trailing edge brushes [8] and porous trailing edges [9]. Porous edges, although more complex than serrations, present greater potential and adaptability. The mitigation of leading or trailing-edge noise using a porous insert is the result of a pressure-release process, resulting in a gradual impedance adjustment instead of an abrupt one between a solid body and the outflow [10]. The same idea has appeared in studies unveiling bio-inspired processes that mimic the silent flight of owls induced by their unique feather structures [11]. Indeed, owls are able to eliminate the self-noise produced during flight by the turbulent pressures in the wing boundary layers and from the legs without being heard by their prey. Such noise reduction relies on the specific plumage of their wings with three main characteristics prone to a silent flight [12]: the leading edge comb-like serrations, the trailing edge fringes and the soft downy material evenly distributed on the top of the wings and over the legs. A number of works has aimed at developing a mimetic surface for the reduction of noise caused by the flow over a surface. To evaluate the separate and combined influences of the fibres flexural elasticity, anisotropy and porosity on the noise reduction, a fibrous structure simulating a compliant but rough surface, much like a soft carpet has been considered [13]. Although a suitable combination of porous materials is a representative configuration, a more detailed characterisation should also include anisotropic fibrous materials [14] and micro-perforated or micro-slit covering membranes [15].

Micro-perforated panels (MPPs) constitute a non-fibrous alternative [16] to conventional silencers when porous components are excluded due, for instance, to the presence of high flow velocity or restrictions imposed by special hygienic conditions, such as in food industries. In addition, they can be made of recyclable materials constituting a non-polluting environmental option. They are tuneable control devices with adjustable performance that can be achieved by a proper selection of their physical constitutive parameters. A number of works [15, 17] have focussed on the study of the acoustic response of MPPs partition in presence of grazing and/or bias flow, with applications to reduced exhaust noise emissions in the transportation industry. Design of the wall-treatments in presence of the flow requires an accurate prediction of their acoustic properties. Computational simulations based on the Lattice-Boltzmann method [17] provides reliable results but they need to be confirmed experimentally. Flow-induced noise measurements are often challenging to perform, as the installation of probes and transducers could alter the porous material properties or be intrusive towards the flow structure. Recently, an experimental investigation concerning the reduction of trailing-edge noise [18] has been conducted for single-stream cold subsonic jets with a round nozzle adjacent to a flat-plate, considering a wide range of flow velocities in an anechoic chamber. Four different materials, with different permeability and roughness were tested to demonstrate the regions of noise reduction in the far field. Other methodologies have considered the use of in-duct aeroacoustic measurements [19] to characterize a micro-perforated absorber in the vicinity of an axial fan.

The main objective of the paper is to compare the influence of testing facilities on the measured aero-acoustic performance of absorbing porous wall-treatments under a low-speed airflow. We aim at examining the role of porosity on the robustness of the aeroacoustic performance of flush-mounted micro-perforated or fibrous materials. The paper is organized as follows. Section 2 describes the two different aeroacoustic testing facilities used for the measurements, low-speed large and small wind tunnels, as well as the microperforated porous samples that have been tested. Section 3 summarizes the aerodynamic properties of the flow structure above the materials. Section 4 compares the flow-induced noise reduction performance of the absorbing materials in both low-speed wind-tunnels. Section 5 examines their ability to reduce source-induced noise under a low-speed flow. A summary of the main results and guidelines for further work is presented in Section 6.

## 2. AEROACOUSTIC TESTINGS

### 2.1 Low-speed large wind tunnel

A first series of measurements have been carried out in an Eiffel-type open large wind-tunnel (LWT) with rectangular test section of width 0.44 m and height 0.56 m, shown in Fig. 1. A fully-developed turbulent boundary layer (TBL) is achieved over the plain rigid ground floor of the test section with mean bulk velocity $U_\infty = 14\,\mathrm{m\,s^{-1}}$, boundary layer thickness 0.071 m and Reynolds number $\mathrm{Re}_x = 2.3\,10^6$. As shown in Fig. 3, a number of absorbing wall-treatments (described in 2.3) have been inserted in the ground floor of the LWT. A pair of nosecone microphones are mounted on a traverse that can be displaced vertically between 4 mm and 72 mm above the samples, but also horizontally by 3 mm upstream the flow direction. A compression driver is laterally flush-mounted 2m upstream of the test section so

that downstream propagation conditions prevail at the sample location.

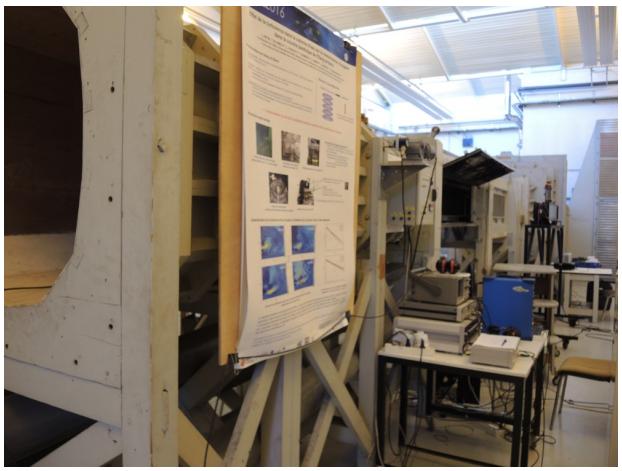

**Figure 1**. Open low-speed large wind-tunnel (LWT) used to characterize the aero-acoustic properties of absorbing wall-treatments under a fully-developed TBL.

### 2.2 Low-speed small wind tunnel

A second series of aeroacoustic measurements have been performed in an open small wind-tunnel (SWT) shown in Fig. 2 from the outlet duct section. The mean bulk velocity is $U_\infty = 16\,\mathrm{m\,s^{-1}}$ and the square test section has a width and height 0.145 m. Unlike in the LWT, the boundary layer at the position of the absorbing wall-treatments has a Reynolds number $\mathrm{Re}_x = 5.3\,10^5$ and is not fully-developed. It is transitional and early developing as it is located after a reattachment zone due to a backward-facing step between the rectangular duct and a box acoustically coupling the convergent to the duct. This flow structure has been characterized from hot-wire anemometric measurements. The aeroacoustic measurements have been performed using a nosecone microphone vertically displaced spanning a zone between 4 mm and 55 mm above the samples. A compression driver, similar to that used in LWT, is flush-mounted on top of the sample location, as shown in Fig. 2.

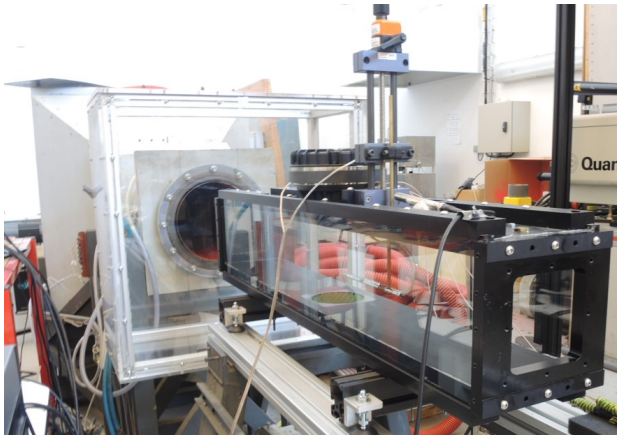

**Figure 2**. Open low-speed small wind-tunnel (SWT) used to characterize the aero-acoustic properties of absorbing wall-treatments under an early-developed boundary layer.

### 2.3 Absorbing wall-treatments

As it can be seen from Fig. 3, four types of absorbing wall-treatments are characterized whose parameters are given in Tables 1 and 2. One considered two micro-perforates MPP1 and MPP2 with perforation ratio 3.2% and 78.5% respectively, both backed by a rigid cylindrical cavity of depth 0.03 m filled with honeycomb core to achieve locally-reacting surface impedance conditions. MPP2 may be coined as an ultra-microperforate due its high density of micro-holes. Unlike MPP1 which was manufactured by mechanical micro-machining, MPP2 has been manufactured by photolithography.

**Table 1.** Micro-perforated panels parameters

| | Hole diameter (mm) | Holes pitch (mm) | Thickness (mm) |
|---|---|---|---|
| MPP1 | 0.5 | 2.5 | 0.5 |
| MPP2 | 0.2 | 0.2 | 0.2 |

Two anisotropic fibrous materials F1 and F2 with both a thickness of 20 mm and low resistivities (below 70 N s $\mathrm{m^{-4}}$) are also tested. F1 is a regular lattice of parallel hard plastic fibers whereas F2 is composed of twisted bio-sourced sisal fibers. Rigidly-backed MPP1 and MPP2 are locally-reacting Helmholtz-type acoustical resonators whereas F2 and F2 are bulk-reacting large radius fibers materials due to the possible occurrence of tangential resonances on the cavity sides.

**Table 2.** Fibrous absorber parameters

| | Porosity (%) | Fiber radius (mm) | Angle (deg) |
|---|---|---|---|
| F1 | 99.8 | 2 | 90 |
| F2 | 97.1 | 0.1 | 62 |

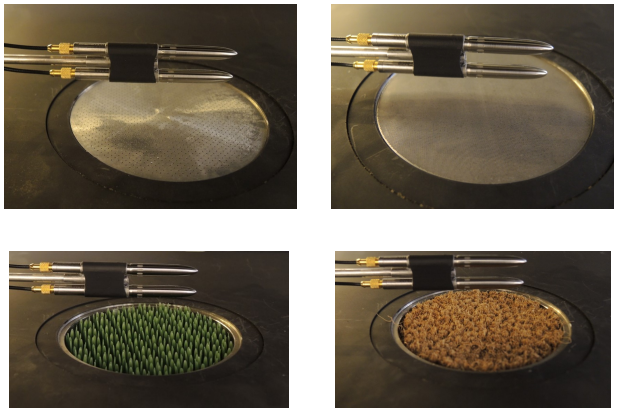

**Figure 3**. Microperforated (MPP1, top left; MPP2: top right) and fibrous (F1, bottom left; F2, bottom right) absorbing wall-treatments, here located in LWT test section with a pair of nosecone microphones.

## 3. AERODYNAMIC PROPERTIES

Anemometric hot-wire measurements of the horizontal velocity have been performed in LWT and SWT above MPP1, MPP2, F1 and F2 to show the influence of the absorbers surface roughness and porosity on the flow mean velocity profile and higher order moments. Figure 4 shows a small variability of the mean flow profiles measured in LWT above the absorbers that stays within 7% with respect to the universal seventh power law valid under a fully-developed TBL (circles in Fig. 4). MPP2 is however constantly underestimating the reference curve which may be due to a transfer of flow momentum through the ultra-porous MPP2 surface. Although the velocity profiles were different due to an early developing boundary layer, the same small variability above each material was also observed in SWT under low free stream velocity.

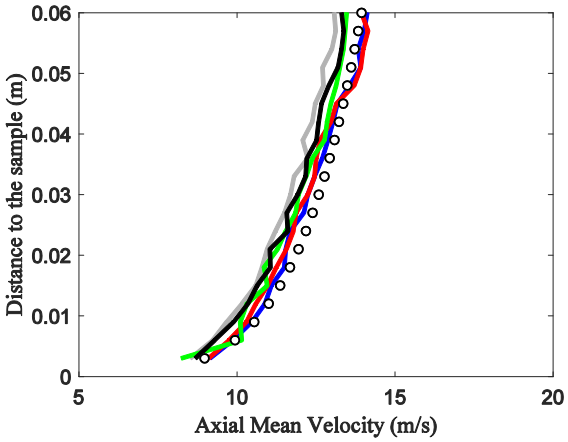


**Figure 4**. Mean velocity profiles measured in LWT above a plain surface (blue), MPP1 (red), MPP2 (grey), F1 (green), F2 (black) and those predicted by the universal power law (circles) under a fully-developed TBL.

In LWT, turbulence rates are ranging from 2% at 0.06 m above all the materials up to 13% (Plain, MPP1, MPP2), 14% (F2) and 17% (F1) at 0.004 m. Turbulent velocity fluctuations are higher within the boundary layer thickness in SWT than in LWT. In SWT, turbulence rates vary between 16% at 0.06 m for all the materials up to 25% (Plain, MPP1, MPP2), 36% (F2) and 38% (F1) at 0.002 m.

## 4. FLOW-INDUCED NOISE REDUCTION

### 4.1 LWT aeroacoustic testings

It is now examined how resonant and fibrous absorbers are able to reduce flow-induced noise induced by a TBL in LWT. Figure 5 shows that MPP1 (resp. MPP2) provide flow-induced noise attenuation by up to 5 dB (resp. 7 dB) between 1.4 kHz and 4.3 kHz (resp. 1.6 kHz and 4.3 kHz). It was found that the maximum attenuation of MPP1 (resp. MPP2) occurs at 2.3 kHz (resp. 3 kHz) over a zone that extends up to 0.04 m (resp. 0.02 m) above MPP1 (resp. MPP2) samples. A moderate flow noise attenuation (1.5 dB) is achieved by F1 between 2.1 kHz and 3.5 kHz, but up to 6dB increase in the SPLs is observed below 1.3 kHz down to 100 Hz due to back-scattering of the wall-pressures over F1 rough surface enhanced by a large porosity. Better flow noise reduction performance are achieved by F2 with up to 5 dB attenuation above 2.4 kHz, with back-scattering

effects lower than those of F1 below 1.3 kHz. Flow noise attenuations stay localized nearby the wall-treatments.

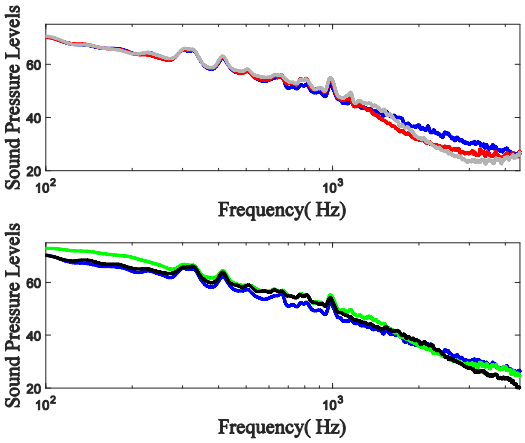


**Figure 5**. Flow-induced noise SPLs measured in LWT (14 m/s) at 4 mm above a plain surface (blue), MPP1 (red), MPP2 (grey), F1 (green), F2 (black) under a fully-developed TBL.

### 4.2 SWT aeroacoustic testings

The aeroacoustic performance of the wall-treatments are now examined in SWT in Fig. 6 and compared to those in LWT shown in Fig. 5 and displayed over the same frequency range.

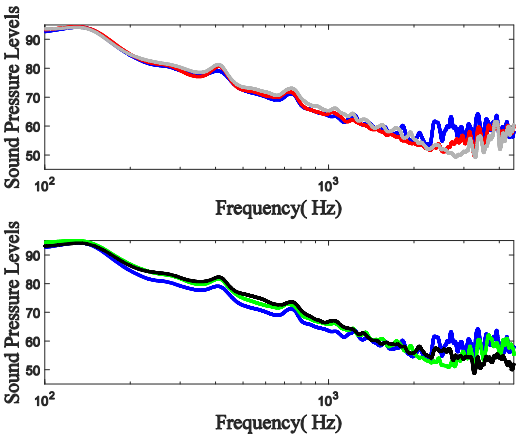


**Figure 6**. Flow-induced noise SPLs measured in SWT (14 m/s) at 3 mm above a plain surface (blue), MPP1 (red), MPP2 (grey), F1 (green), F2 (black) under an early-developed boundary layer.

It can be seen from Fig. 6 that reduced efficiency ranges for flow noise reduction in SWT is observed above the micro-perforated wall-treatments with respect to LWT, but with greater maximum attenuation, namely 8 dB between 1.6 kHz and 3 kHz for MPP1 and 10 dB between 2.3 kHz and 3.8 kHz for MPP2. Greater flow noise reductions are achieved by F1 (up to 9 dB between 2.2 kHz and 3.3 kHz) and by F2 (up to 10 dB above 2.4 kHz) in their efficiency range in SWT when compared to those in LWT. But flow-noise enhancement by F1 (resp. F2) is also observed below 1.3 kHz, although to a lesser extent when compared to LWT measurements. The most performant wall-treatments for flow-induced noise reduction with least flow noise generation appear to be MPP2 and F2.

## 5. SOURCE-NOISE REDUCTION UNDER A LOW-SPEED FLOW

### 5.1 Source-noise reduction in LWT

The compression drivers mounted on the wind-tunnels are now switched on to generate white noise over the bandwidth 100 Hz – 5 kHz. The source-noise reduction performance of the wall-treatments under a low-speed flow in LWT are shown in Figs. 7 and 8. Overall, one retrieves the efficiency ranges as well as the maximum attenuation performance which stay consistent with the results presented in Section 4.

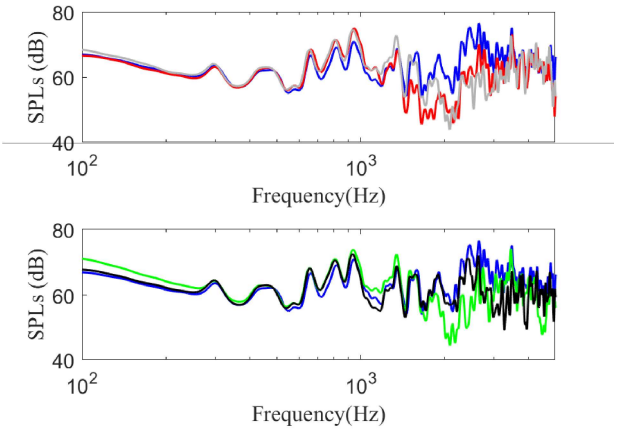


**Figure 7**. SPLs induced by an upstream source in LWT (14 m/s) at 3 mm above a plain surface (blue), MPP1 (red), MPP2 (grey), F1 (green), F2 (black) under a fully-developed TBL.

MPP1 brings up to 10 dB attenuation between 1.4 kHz and 3 kHz with a Helmholtz-type resonance frequency whereas MPP2 reaches up to 18 dB attenuation between 1.6 kHz and 3.5 kHz with the largest attenuation obtained nearby the Helmholtz-type resonance frequency of the absorbers, namely at 1.7 kHz for MPP1 and at 3 kHz for MPP2. As for the fibrous treatments, F1 achieves up to 12 dB source noise attenuation between 1.7 kHz and 3 kHz and F2 also realizes maximum 12 dB noise reduction but at higher frequencies, between 2.3 kHz and 4 kHz.

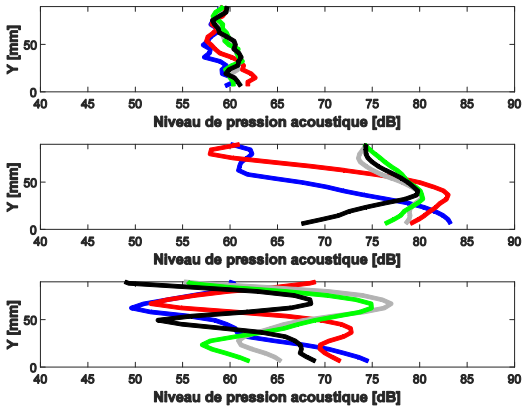


**Figure 8**. SPLs profiles induced by an upstream source in LWT (14 m/s) at 400 Hz (top), 2.7 kHz (middle) and 4.7 kHz (bottom) above a plain surface (blue), MPP1 (red), MPP2 (grey), F1 (green), F2 (black) under a fully-developed TBL.

The following ordering, MPP1 – F1 – MPP2 – F2 holds, when classified by increasing values for the central frequencies of the efficiency bandwidth. However, risks of flow-induced noise generation may occur below 300 Hz over F1 sample. Figure 8 shows that these relative performance are localized within the TBL boundary layer thickness, e.g. up to 0.04 m above the samples. In order to achieve source-induced noise reduction over an extended cross-section area, a larger treatment surface would be required.

### 5.2 Source-noise reduction in SWT

It is clear from Fig. 9 that the classification proposed in Sec. 5.1 still holds in SWT as for the efficiency frequency ranges of the samples. The attenuation is however hindered by a pressure node that occurs at 2.3 kHz, e.g. within the efficiency range of all the samples except F2.

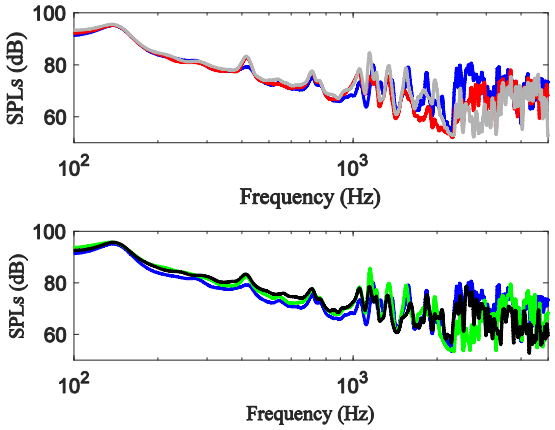


**Figure 9**. SPLs induced by a top source in SWT (14 m/s) at 3 mm above a plain surface (blue), MPP1 (red), MPP2 (grey), F1 (green), F2 (black) under an early-developed boundary layer.

It can be seen from Fig. 10 that the samples attenuation effects are observed over a larger cross-sectional area of the SWT with respect to the LWT. For instance, it occurs at 2.7 kHz up to 0.05 m above the samples in SWT, e.g. over 60% of the SWT duct cross-section with respect to only 10% in LWT. This is due to a greater treated area ratio over the bottom wall of the test sections, namely 38% in the SWT compared to 12% in the LWT.

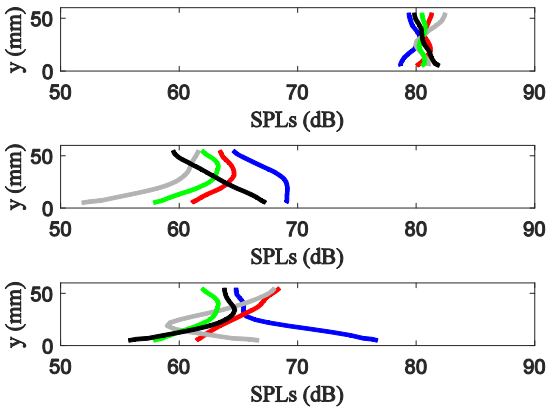


**Figure 10**. SPLs profiles induced by a top source in SWT (14 m/s) at 400 Hz (top), 2.7 kHz (middle) and 4.7 kHz (bottom) above a plain surface (blue), MPP1 (red), MPP2 (grey), F1 (green), F2 (black) under an early-developed boundary layer.

### 5.3 Intensity profiles above the absorbers

Neglecting low-speed flow convective effects, the horizontal ($x$) and vertical ($y$) components of the acoustic intensity read $I_{x,y} = 0.5\,\mathrm{Re}\left[S_{pv_{x,y}}\right]$, approximated by $I_{x,y} \approx \left(2\omega\rho_0 dl_{x,y}\right)^{-1}\mathrm{Re}\left[S_{pp^{+}_{x,y}} - S_{pp^{-}_{x,y}}\right]$ (from Euler equation) in terms of the cross-spectral densities between the acoustic pressures $p$ and $p^{\pm}_{x,y}$ measured at $dl_{x,y} = 3$ mm apart from $p$ along the $x$- or $y$-directions, $\omega$ being the angular frequency and $\rho_0$ the air density.

Figure 11 shows that the acoustic intensity fluxes measured in LWT at 2kHz above MPP1, MPP2 and F1 increase as $y \to 0$ and point essentially towards the absorbing samples surface, in accordance with the noise reduction performance shown in Fig. 7 for these materials. F2 is less performant at 2 kHz due to a scatter between the $I_x$ and $I_y$ components towards $y = 0$. For the plain rigid case, $I_y = 0$ towards $y = 0$ due to zero-normal velocity over the rigid surface. This is also observed in Fig. 12 over a more extended area above SWT rigid surface.

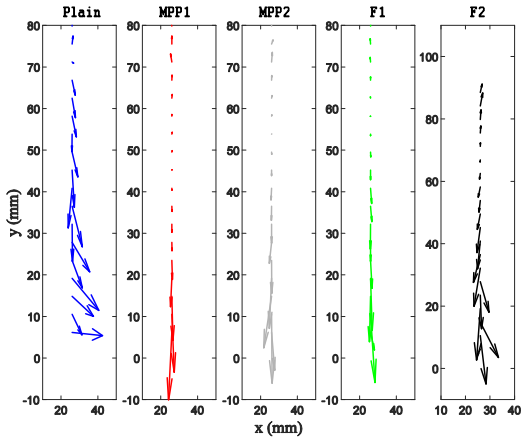


**Figure 11**. Acoustic intensity profiles induced by an upstream source in LWT (14 m/s) at 2 kHz above a plain surface (blue), MPP1 (red), MPP2 (grey), F1 (green), F2 (black) under a fully-developed TBL.

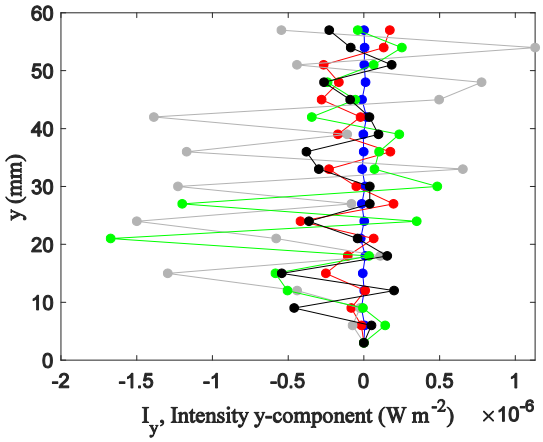


**Figure 12**. Profiles of the vertical acoustic intensity induced by a top source in SWT (14 m/s) at 3 kHz above a plain surface (blue), MPP1 (red), MPP2 (grey), F1 (green), F2 (black) under an early-developed boundary layer.

Figure 12 also shows significant vertical fluxes of acoustical intensity at 3 kHz, by decreasing order of magnitude, above the samples MPP2, F1, F2 and MPP1, when inserted in SWT test section. This complies with the SPL source-induced noise reduction shown in Fig. 9 at 3 kHz.

## 6. CONCLUSIONS

This study assessed the variability of the aeroacoustic performance of micro-perforated and fibrous wall-treatments with respect to low-speed wind-tunnel testing facilities. They do not substantially modify the mean-flow velocity profile, except F1, prone to generate flow-induced noise. MPP2 and F2 are the most performant wall-treatments for flow-induced noise reduction in LWT and SWT. The wideband efficiency range for source noise reduction in LWT or SWT is consistently shifted up in frequency when considering MPP1 – F1 – MPP2 – F2, respectively. Such noise reductions are observed in the vicinity of the treatment in LWT whereas they occur over an extended cross-sectional area in SWT. These absorbing properties are supported by acoustic intensity measurements that show large acoustic fluxes pointing towards the most absorbent materials. More insights would be gained on the flow-surface interactions and the reduction of flow-induced noise from numerical aero-acoustic simulations such as Lattice Boltzmann Modelling.

## 7. ACKNOWLEDGMENTS

This work is part of the project TED2021-130103B-I00, funded by MCIN/AEI/10.13039/501100011033 and the European Union "NextGenerationEU"/PRTR. It has been supported from the French government under the France 2030 investment plan, as part of the Initiative d'Excellence d'Aix-Marseille Université - A*MIDEX (AMX-19-IET-010).

## 8. REFERENCES

[1] J. F. Williams and L. Hall, "Aerodynamic sound generation by turbulent flow in the vicinity of a scattering half plane", Journal of Fluid Mechanics, vol. 40, pp. 657–670, 1970.

[2] F. Barbosa, "Ultra High Bypass Ratio Engine Technology Review - The Efficiency Frontier for the Turbofan Propulsion," SAE Technical Paper 2021-36-0032, 2022.

[3] W. Y. Liu, "A review on wind turbine noise mechanism and de-noising techniques", Renewable Energy, vol. 108, pp. 311–320, 2017.

[4] J. Kang and M. W. Brocklesby, "Feasibility of applying micro-perforated absorbers in acoustic window systems," Applied Acoustics, vol. 66, pp. 669–689, 2005.

[5] E. Garnell, M. Åbom and G. Banwell, "The use of the two-port method to characterize high-speed small fans", Applied Acoustics, vol. 146, pp. 155–163, 2019.

[6] S. Oerlemans, M. Fisher, T. Maeder and K. Kögler, "Reduction of wind turbine noise using optimized airfoils and trailing edge serrations", AIAA Journal, vol. 47, pp. 1470–1481, 2009.

[7] T. Lutz, A. Herrig, W. Würz, M. Kamruzzaman and E. Krämer, "Design and wind-tunnel verification of low-noise airfoils for wind turbines", AIAA Journal vol. 45(4), pp. 779–785, 2007.

[8] A. Finez, E. Jondeau, M. Roger, and M. C. Jacob. "Broadband noise reduction with trailing edge brushes". AIAA 2010-3980, 16th AIAA/CEAS Aeroacoustics Conference, Stockholm, Sweden, 07-09 June 2010.

[9] T. Geyer, E. Sarradj, and C. Fritzsche, "Measurement of the noise generation at the trailing edge of porous airfoils", Experiments in Fluids, vol. 48, pp. 291–308, 2010.

[10] C. Teruna, Aerodynamic Noise Reduction with Porous Materials: Aeroacoustics Investigations and Applications. PhD. Thesis, TU Delft Library, 2022.

[11] G. Lilley, "A study of the silent flight of the owl, Proceedings of the 4th AIAA/CEAS Aeroacoustics Conference", AIAA 1998-2340, Toulouse, France, 02-04 June 1998.

[12] T. F. Geyer, V. T. Claus, E. Sarradj, J. W. Jaworski and P. M. Markus, "Silent owl flight: the effect of the leading edge comb on the gliding flight noise", Proceedings of the 22nd AIAA/CEAS Aeroacoustics Conference, AIAA 2016-3017, Lyon, France, 30 May - 01 June 2016.

[13] I. A. Clark, C. Daly, W. Devenport, W. N. Alexander, N. Peake, J. W. Jaworski and S. Glegg, "Bio-inspired canopies for the reduction of roughness noise", Journal of Sound and Vibration, vol. 385, pp. 33–54, 2016.

[14] T. Bravo and C. Maury, "Sound absorption by thin micro-perforated partitions lined with anisotropic fibrous materials", Journal of Sound and Vibration, vol. 417, pp. 165–181, 2018.

[15] T. Bravo, C. Maury, and C. Pinhède, "Absorption and transmission of boundary layer noise through flexible multi-layer micro-perforated structures," Journal of Sound and Vibration, vol. 395, pp. 201-223, 2017.

[16] D. Y. Maa, "Potential of microperforated panel absorbers", Journal of the Acoustical Society of America, vol. 104, pp. 2861–2866, 1998.

[17] C. Maury, T. Bravo, and D. Mazzoni, "The use of microperforations to attenuate the cavity pressure fluctuations induced by a low-speed flow," Journal of Sound and Vibration, vol. 439, pp. 1-16, 2019.

[18] H. K. Jawahar, S. A. Karabasov and M. Azarpeyvand, "Jet installation noise reduction using porous treatments", Journal of Sound and Vibration, vol. 545, pp. 117406, 2023.

[19] F. Czwielong, S. Floss, M. Kaltenbacher and S. Becker, "Influence of a micro-perforated duct absorber on sound emission and performance of axial fans", Applied Acoustics, vol. 174, pp. 107746, 2021.